coatings

MDPI

Article

# A Rapid Surface-Enhanced Raman Scattering (SERS) Method for $Pb^{2+}$ Detection Using L-Cysteine-Modified Ag-Coated Au Nanoparticles with Core–Shell Nanostructure

**Zhou Xu [1,*], Linwei Zhang [1], Bo Mei [1], Jia Tu [2], Rong Wang [1], Maolong Chen [1] and Yunhui Cheng [1,*]**

1 School of Chemistry and Biology Engineering, Changsha University of Science & Technology, Changsha 410114, China; 18508464416@163.com (L.Z.); mebal1990@163.com (B.M.); wrsmbxfdbz@163.com (R.W.); mlchen@xmu.edu.cn (M.C.)

2 Hunan Academy of Forestry, Changsha 410004, China; tujia469@hotmail.com

* Correspondence: xz_jnu@126.com (Z.X.); chengyh6488@gmail.com (Y.C.); Tel.: +86-731-8525-8322 (Z.X.)

Received: 20 September 2018; Accepted: 7 November 2018; Published: 10 November 2018


**Abstract:** A rapid surface-enhanced Raman scattering (SERS) method for $Pb^{2+}$ detection has been developed based on L-cysteine-modified Ag-coated Au nanoparticles with core-shell nanostructure. Specifically, L-cysteine-functionalized Au@Ag core-shell probes bearing Raman-labeling molecules (4-ATP) are used to detect $Pb^{2+}$ upon the formation of nanoparticle aggregates. The proposed SERS-based method shows a linear range between 5 pM and 10 nM, with an unprecedented limit of detection (LOD) of 1 pM for $Pb^{2+}$; this LOD shows the method to be a few orders of magnitude more sensitive than the typical colorimetric approach that is based on the aggregation of noble metal nanoparticles. Real water samples diluted with pure water have been successfully analyzed. This SERS-based assay may provide a general and simple approach for the detection of other metal ions of interest, and so could have wide-ranging applications in many areas.

**Keywords:** surface-enhanced Raman scattering; Ag-coated Au nanoparticles; $Pb^{2+}$; detection

## 1. Introduction

Some metal ions are essential for normal physical activities of humans, whereas others may be harmful to health [1]. $Pb^{2+}$, accumulated strongly in the food chain, is one of the most toxic heavy metal ions and it poses a significant risk to human health, potentially causing heart failure, abdominal pain, high blood pressure, and cancer, even after a minute exposure [2–4]. According to the Environment Protection Agency (EPA) guidelines, $Pb^{2+}$ concentrations must not exceed 50 μg $L^{-1}$ in drinking water [5].

Conventional analytical techniques applied to detect $Pb^{2+}$ sensitively and selectively are based on atomic absorption spectrometry (AAS) [6,7], inductively coupled plasma mass spectrometry (ICP-MS) [8], X-ray fluorescence spectrometry (XRF) [9], and chromatography [10]. These methods have demonstrated good sensitivity, but some of them involve a pre-treatment step and are thus rather time-consuming. To overcome these disadvantages, different sensors have been used for $Pb^{2+}$ detection, based on DNAzyme [11], fluorophores [12], oligonucleotides [13], and nanomaterials [14]. However, these methods are complex and unstable, with delayed responses to $Pb^{2+}$.

Recently, surface-enhanced Raman scattering (SERS) has shown significant superiority in terms of non-invasiveness for trace and ultra-trace detection in food analysis and bioassays [15,16]. Noble/precious metal nanoparticles have typically been deployed as SERS substrates, such as

nanospheres [17], nanostars [18], nanorods [19], and nanopillars [20]. In order to improve the applicability of SERS, a great deal of effort has been made to increase the enhancement factor. Previous reports have indicated that the metallic nanoparticles are usually coated with a dielectric nanolayer for SERS enhancement. The LSPR (localized surface plasmon resonance) features will be altered by the dielectric layer, which will have a different dielectric constant from the surrounding medium.

In the present study, we have constructed a platform of Ag-coated Au nanoparticles (Au@Ag core-shell) for the ultrasensitive detection of $Pb^{2+}$ utilizing the excellent sensitivity of SERS. Au@Ag NPs that were functionalized with L-cysteine were prepared. In the presence of the target metal ions of $Pb^{2+}$, these will be coordinated by the glycine residues of the L-cysteine moieties on the surface of the Ag-coated nanoparticles. This coordination results in the formation of a so-called "inner complex salt", a type of coordination compound that is electrically neutral and highly stable, as illustrated in Scheme 1. In the Au@Ag bimetallic nanostructures, the Ag layer is mainly coated on the surface of the cores, which leads to a change in SERS activity. The Raman intensity increases linearly with the logarithmic concentration of $Pb^{2+}$ ranging from $5 \times 10^{-12}$ to $1 \times 10^{-8}$ M, with a detection limit of $1 \times 10^{-12}$ M. This method based on SERS for the detection of harmful substances in food has an obviously higher sensitivity when compared to ordinary colorimetric [10], fluorescence [21], and electrochemical methods [22].

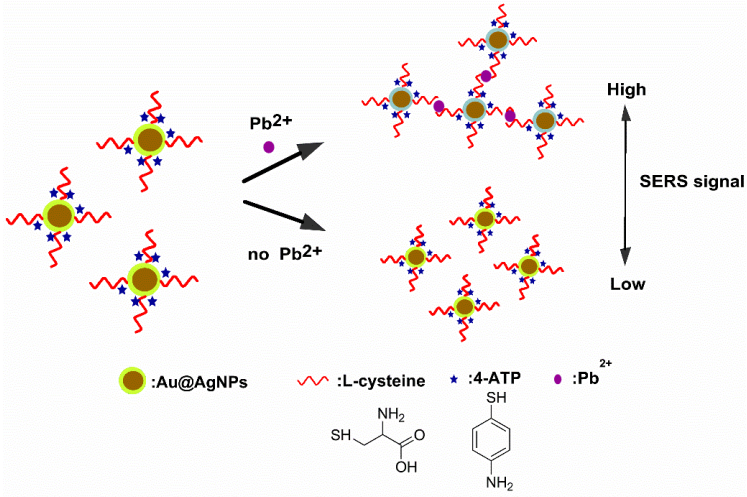


**Scheme 1.** Schematic illustration of the detection of $Pb^{2+}$ based on the aggregation of Au@Ag nanoparticles.

## 2. Materials and Methods

### *2.1. Materials*

Trisodium citrate, sodium citrate, chloroauric acid ($HAuCl_4$), silver nitrate ($AgNO_3$), L-cysteine (L-cys), 4-aminothiophenol (4-ATP), and potassium thiocyanate (KSCN) were purchased from J&K Scientific Ltd. (Guangzhou, China). The metal ion standards used ($Pb^{2+}$, $Hg^{2+}$, $Cu^{2+}$, $Cd^{2+}$, $Zn^{2+}$, $Cr^{2+}$, $Ni^{2+}$, $Co^{2+}$, $As^{2+}$) were purchased from the National Institute of Metrology P. R. C. (Beijing, China). All of these reagents were used without further treatment. All of the solutions were prepared with ultrapure water ($\geq$18 MΩ, Milli-Q, Millipore, MA, USA).

### *2.2. Instruments*

The size distributions of Au@Ag NPs were measured with a Zetasizer Nano ZS system (633 nm laser, Malvern Instruments, Malvern, UK). Transmission electron microscopy (TEM) images were obtained on a JEOL JEM-2100 instrument (Tokyo, Japan) operating at an acceleration voltage of 200 kV. Raman spectra were obtained from a liquid cell using a LabRam-HR800 micro-Raman spectrometer (Jobin Yvon, Paris, France) with Lab-spec 5.0 software and an air-cooled He-Ne laser with a power of

~8 mW for 532.8 nm excitation, using a 50× objective lens. All spectra presented herein were acquired through a 50 s accumulation.

### 2.3. Synthesis of Au@Ag NPs

Au@Ag NPs were synthesized according to a previously published seed-mediated growth method [23]. Specifically, they were prepared through a two-step reduction method that involved the synthesis of 10 nm Au cores and the subsequent growth of 15 nm Ag shells. Au NPs with a diameter of 10 nm were synthesized by reduction of $HAuCl_4$ using trisodium citrate. Briefly, an aqueous solution of $HAuCl_4$ (0.25 mM, 100 mL) was brought to a reflux while vigorous stirring, and then trisodium citrate solution (1% *w*/*w*, freshly prepared; 2.0 mL) was added quickly to the boiling mixture. After reacting for three minutes, the color of the solution changed from blue to wine-red. After keeping the solution under reflux for a further 15–30 min, the heat source was removed to allow the reaction solution to cool to room temperature. The 10 nm Au NPs were thereby obtained. An aliquot (200 µL) of the above AuNP colloid was then mixed with $AgNO_3$ (3 mM, 20 µL) and ascorbic acid (0.1 M, 10 µL) under magnetic stirring. $AgNO_3$ was reduced by ascorbic acid and the resultant Ag continuously grew on the surfaces of the Au seeds. After the wine-red solution turned orange, it was continuously stirred for a further 30 min to obtain an Au@Ag NPs colloid. Finally, this Au@Ag NPs colloid was twice concentrated to dryness by centrifuging at 6950 g for 15 min, and the solid was re-suspended with 10 mL ultrapure water. The Au@Ag NPs were stored in a refrigerator at 4 °C prior to use.

### 2.4. Synthesis of Au@Ag NPs Probes

Au@Ag NP probes were synthesized directly by an Ag-S bond-forming method. Firstly, freshly prepared L-cysteine solution (6 µL) was added to 4 nM Au@Ag NPs aqueous suspension (100 µL) for 3 h to give a final concentration of 60 nM. A solution of the Raman label 4-aminothiophenol in ethanol (freshly prepared) with a final concentration of 2 µM was then added to the system under stirring. The mixture was allowed to react for 12 h at room temperature to afford Au@Ag NP conjugates, which served as probes in subsequent experiments.

### 2.5. SERS Assay for $Pb^{2+}$ Detection

The SERS detection of $Pb^{2+}$ in aqueous solution was performed at room temperature. Briefly, aliquots (10 µL) of aqueous $Pb^{2+}$ solutions of various concentrations were added to portions (100 µL) of an aqueous suspension of Au@Ag NPs probes and were diluted to 200 µL with ultrapure water. After standing for 30 min, the products were placed with a cuvette and characterized by Raman spectroscopy. The spectral response range of the Raman spectrometer was 400–1800 $cm^{-1}$. Each experiment was performed in triplicate.

### 2.6. Specificity Analysis

The specificity of our SERS probe was evaluated by determining another eight relevant metal ions, namely $Hg^{2+}$, $Cu^{2+}$, $Cd^{2+}$, $Zn^{2+}$, $Cr^{2+}$, $Ni^{2+}$, $Co^{2+}$, and $As^{2+}$. Solutions of these metal ions at 100 ng $mL^{-1}$ (containing 1 µM KSCN) and 1 ng $mL^{-1}$ $Pb^{2+}$ (containing 1 µM KSCN) were added to 100 µL portions of the Au@Ag NPs suspension. The other procedures of the specific experiments were the same as those for $Pb^{2+}$ detection. Each experiment was performed in triplicate.

### 2.7. Recovery of $Pb^{2+}$ Spiked in Drink Water Samples

To verify the feasibility and practicability of this method, drinking water was purchased from a local supermarket in Hunan. It was confirmed to test negative for $Pb^{2+}$. In the spiked experiments, 10 µL $Pb^{2+}$ standard solution (1 nM and 10 nM) was added to 90 µL of the drink water sample (as the spiked final $Pb^{2+}$ concentration of 0.1 nM and 1 nM), respectively. Then, 100 µL of Au@Ag NPs probe was added into the spiked samples (100 µL) for reacting 30 min. After that, the reacted solution

was placed with a cuvette (1 cm) and was characterized by Raman spectroscopy. The detected $Pb^{2+}$ concentration was calculated from the standard linear equation by the obtained ΔRaman Intensity at 1582 $cm^{-1}$ with various spiked concentration, which was used for the calculation of the recovery to verify the practical detection performance of the SERS sensor.

## 3. Results

### *3.1. Detection Rationale*

Scheme 1 depicts the detection rationale of the present approach for ultrasensitive SERS detection of $Pb^{2+}$ based on Au@Ag NPs. The designed SERS sensor relies on the Raman intensity at 1582 $cm^{-1}$ increasing linearly with increasing $Pb^{2+}$ concentration. After preparing Au@Ag NPs as described above, L-cys and 4-ATP were appended on their surfaces through Ag–S bonds. L-Cys provides a –COOH group and an $–NH_2$ group to chelate heavy metal ions [24,25]. Thus, L-Cys can capture added $Pb^{2+}$ in aqueous solution, resulting in the aggregation of the Au@Ag NPs, leading to Raman "hot spots" with markedly enhanced SERS signals. The degree of aggregation of the Au@Ag NPs is strongly dependent on the concentration of $Pb^{2+}$.

### *3.2. Establishment of the SERS-Based Aptasensor for $Pb^{2+}$ Detection*

The size distribution and morphology of the nanocomposites were examined by means of transmission electron microscopy (TEM) and dynamic light scattering (DLS). As shown in Figure 1A, the newly prepared Au@Ag NPs showed an average hydrodynamic diameter of about 25.5 nm. The DLS diameter of AuNPs is slightly larger than the dimensions that were obtained by TEM, which is consistent with previous published papers [26,27]. The hydrodynamic diameter of the Au@Ag NPs probe was larger than that of the Au@Ag NPs (Figure 1B). Moreover, no aggregation was evident (Figure 1E), demonstrating that our Au@Ag NP probes had been successfully synthesized. Following the addition of $Pb^{2+}$ (1 nM), the Au@Ag NPs probes would be aggregated due to chelation of the analyte by the surface-bound L-Cys groups (Figure 1F). Indeed, the average hydrodynamic diameter of the Au@Ag NP probe aggregates in the presence of $Pb^{2+}$ showed a marked increase from 42.51 nm (Figure 1B) to 136.3 nm (Figure 1C), supporting the proposed mechanism. The TEM images are consistent with the DLS data (Figure 1D–F).

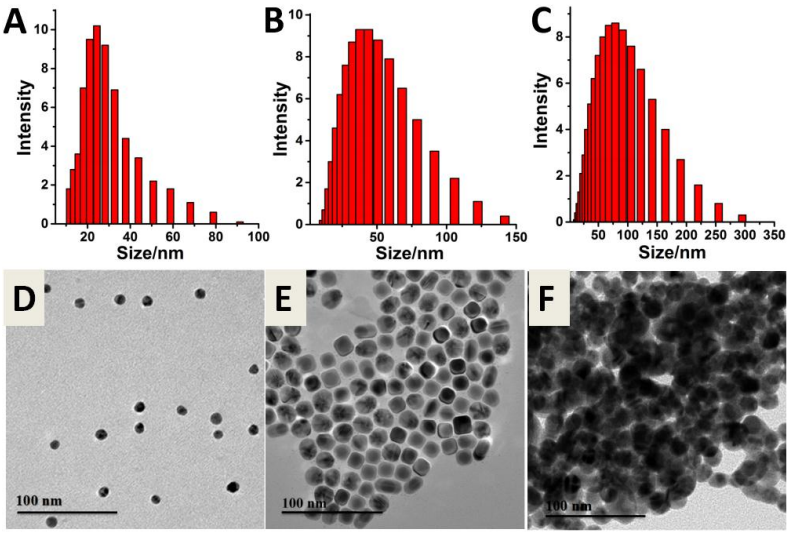


**Figure 1.** Mean average hydrodynamic diameters of (**A**) Au@Ag NPs, (**B**) Au@Ag NPs probes and (**C**) Au@Ag NPs probes aggregations in the presence of $Pb^{2+}$. Transmission electron microscopy (TEM) of (**D**) Au@Ag NPs and (**E**) Au@Ag NPs probes and (**F**) Au@Ag NPs probes aggregations in the presence of $Pb^{2+}$.

As summarized in Figure 2, the LSPR bands of the Au NPs and Au@Ag core/shell NPs were different. The LSPR band of 13 nm Au NPs was located at around 520 nm, but was blue-shifted after coating with Ag shells. A new LSPR band attributable to the Ag shells appeared at around 391 nm, which steadily increased as the Ag shell thickness increased. To evaluate the stability of the developed method, the SERS activity was measured over 15 days (Figure S1). The SERS activity of the probes was still maintained by >80% after 15 days. These results confirmed that the SERS probes proposed the satisfactory stability.

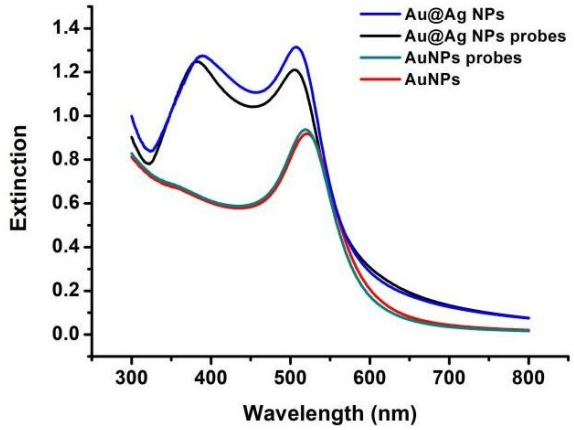


**Figure 2.** Extinction spectra of Au NPs, AuNPs probes, Au@Ag NPs, and Au@Ag NPs probes.

As shown in Figure 3, the SERS reporter group 4-ATP exhibited two main Raman bands: ν(C–S) at 1075 $cm^{-1}$ and ν(C–C) at 1582 $cm^{-1}$, as previously reported by Wang et al. [28] and Kim et al. [29]. In order to verify SERS enhancement with the Ag-coated Au NPs, the Raman spectra of 4-ATP under different conditions were measured. From Figure 3, the absolute values of SERS intensities increased in the order AuNPs < Au@Ag NPs < AuNP aggregates < Au@Ag NP aggregates. The Raman signal of Au@Ag NP aggregates ($C_{Pb}{}^{2+}$ = 5 nM) was strikingly higher than that of the Au NP aggregates at 1582 $cm^{-1}$, demonstrating enhanced SERS activity through the local electric field enhancement of the Au-Ag bimetallic nanoshell [30]. The value of SERS analytical enhancement factors (AEF) of Au@AgNPs aggregation is 5.5-fold than that of aggregation AgNPs.

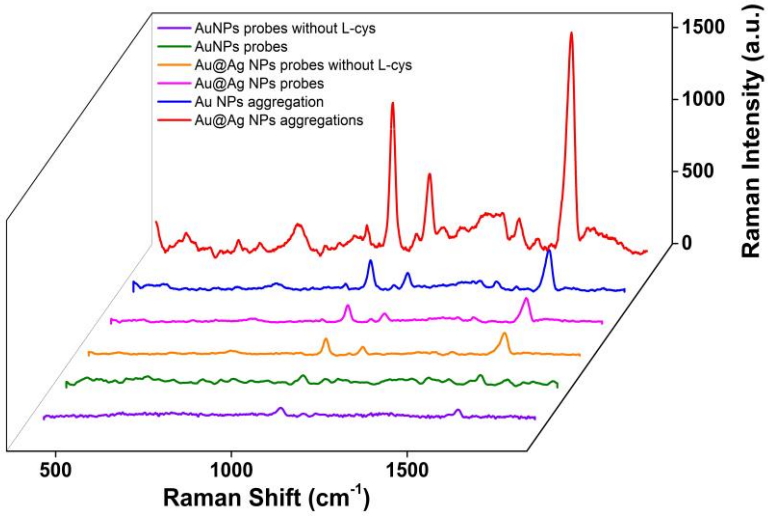


**Figure 3.** Raman spectra of Au NPs probes, Au NPs probes without L-cys, Au@Ag NPs probes, Au@Ag NPs probes without L-cys, Au NP aggregates, and Au@Ag NP aggregates.

To evaluate the interaction between surface-bound L-cysteine and $Pb^{2+}$, the functionalized Au@Ag NP probes were mixed with different concentrations of $Pb^{2+}$. As clearly shown in Figure 4A, the Raman intensity of the SERS probe at 1582 $cm^{-1}$ was gradually increased with an increasing concentration of $Pb^{2+}$ from 5 pM to 10 nM, owing to the increase in "hot spots". This directly confirmed the chelation of $Pb^{2+}$ by surface-bound L-cys. Figure 4B shows a linear standard curve obtained by plotting the intensity of the 1582 $cm^{-1}$ peak against the logarithm of the concentration of $Pb^{2+}$ in the range from 5 pM to 10 nM, which more clearly revealed the increase in SERS signal intensity. The standard curve showed a good linear relationship, with a correlation coefficient of 0.9988 and a limit of detection (LOD) of 1 pM for $Pb^{2+}$ ions. When compared with the conventional UV-Vis spectroscopy method, the sensitivity of this method increased by 3–4 orders of magnitude [31].

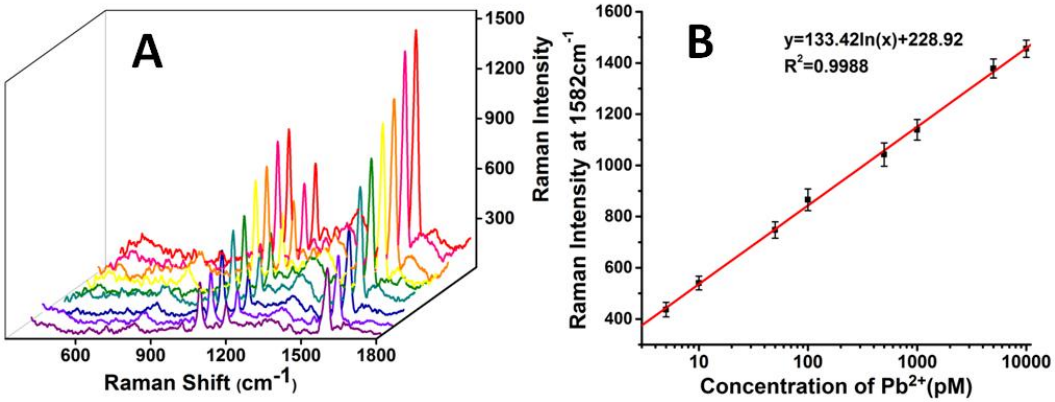


**Figure 4.** (**A**) Surface-enhanced Raman scattering (SERS) spectra of 4-ATP in the presence of $Pb^{2+}$ at different concentrations, from front to back: 0, 0.005, 0.01, 0.05, 0.1, 0.5, 1, 5, 10 nm. (**B**) Linear plot of intensity of the 1582 $cm^{-1}$ peak versus the $Pb^{2+}$ concentration.

### *3.3. Selectivity of the SERS Probe for $Pb^{2+}$*

The selectivity of this method was also quantified by testing the response of the functionalized Au@Ag NP probes to the presence of other potentially interfering metal ions, namely $Hg^{2+}$, $Cu^{2+}$, $Cd^{2+}$, $Zn^{2+}$, $Cr^{2+}$, $Ni^{2+}$, $Co^{2+}$, and $As^{2+}$. According to the stability constant (lg βn) between the masking agent and the metal ions, we can choose the proper masking agent to improve the selectivity of the SERS sensor. Stability constant is equilibrium constant for the formation of a complex in solution [32]. It is a measure of the ability of the interaction between the masking agent and the metal ions to form the complex [33]. The lg βn of $SCN^-$ with $Hg^{2+}$, $Cu^{2+}$, $Cd^{2+}$, $Zn^{2+}$, $Cr^{2+}$, $Ni^{2+}$, $Co^{2+}$, and $Pb^{2+}$ is 21.70, 12.11, 3.6, 2.00, 2.98, 1.81, 1.82, and 1.00, respectively [34]. Indeed, the stability constant of lg βn with $Pb^{2+}$ is as low as 1.00. It indicates the $SCN^-$ could form more stable coordination compounds with other metal ions than that of $Pb^{2+}$, thereby other metal ions for combining $SCN^-$ cannot recognize L-cys appended on Au@Ag NPs surfaces in the detection system, which reduce the concentration of free other metal ions. Thus, we chose KSCN as a masking agent. Figure 5 clearly illustrates that the Raman intensity of 4-ATP at 1582 $cm^{-1}$ was the strongest only when the SERS probe was incubated with $Pb^{2+}$. The other ions induced insignificant changes in the Raman signal of 4-ATP at 1582 $cm^{-1}$. It is well known that the Raman intensity is closely linked with the aggregation level of functionalized Au@Ag NPs. Clearly, the tested metal ions (other than $Pb^{2+}$) did not induce remarkable SERS signal changes (in the presence of KSCN) in the detection system. When comparing with previous similar work [35,36], the SERS sensors have an excellent selectivity for $Pb^{2+}$.

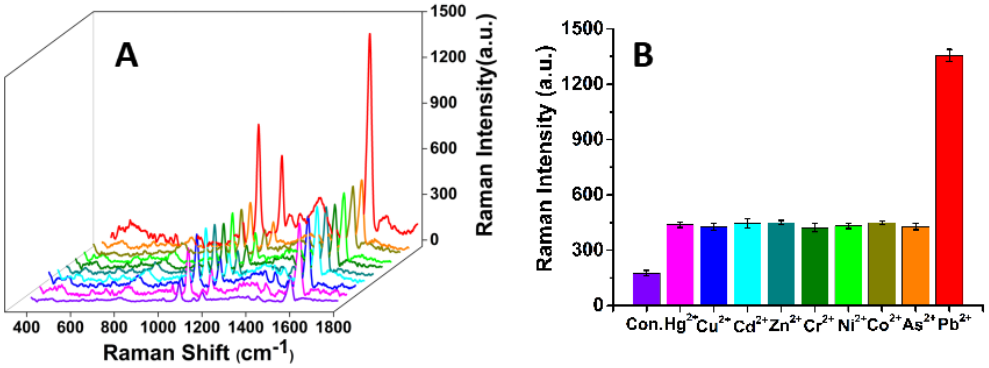


**Figure 5.** Specificity test with various metal ions. (**A**) SERS spectra of 4-ATP in the presence of different metal ions; the concentration of $Pb^{2+}$ was 1 ng $mL^{-1}$, whereas for the other metal ions it was 100 ng $mL^{-1}$. (**B**) Bar chart based on the Raman intensities at 1582 $cm^{-1}$.

### *3.4. Recovery of $Pb^{2+}$ Spiked in Water Samples*

To evaluate the feasibility of applying the designed SERS-based sensor, recovery tests were performed at two spiking levels of $Pb^{2+}$ (0.1 and 1 nM). The recoveries of $Pb^{2+}$ were in the range 96.2%–103.5%. The relative standard deviations (RSD) were less than 0.47%–0.62% for the targets tested, as shown in Table 1. Each extraction was performed in triplicate. The results confirmed that this ultrasensitive SERS detection method that was based on Au@Ag NPs could successfully be used as a screening tool for $Pb^{2+}$ residues in drinking water.

**Table 1.** Determination of $Pb^{2+}$ spiked in drinking water.

| Sample | Spiked Concentration (nM) | Detected Concentration (nM) | RSD (%) ($n$ = 5) | Recovery (%) ($n$ = 5) |
|---|---|---|---|---|
| Drinking water | 0.1 | 0.0962 | 0.47 | 96.2 |
| | 1.0 | 1.0350 | 0.62 | 103.5 |

## 4. Conclusions

In summary, we have successfully developed an ultrasensitive SERS detection method for $Pb^{2+}$ based on Au@Ag NP probes. The sensing strategy for $Pb^{2+}$ ions is based on the interaction between surface-bound L-cysteine and $Pb^{2+}$. With this SERS sensor, highly sensitive and selective recognition of $Pb^{2+}$ in aqueous solution, with a detection limit of 1 pM, was accomplished. We believe that this SERS sensor may provide a potential method for $Pb^{2+}$ ion detection in food safety and other applications.

**Supplementary Materials:** The following are available online at http://www.mdpi.com/2079-6412/8/11/394/s1, Figure S1: The stability and life-time of the Au@Ag NPs probes; Figure S2: Statistical diameters of Au NP, Au@Ag NP according to TEM image.

**Author Contributions:** Conceptualization, Z.X. and Y.C..; Methodology, L.Z.; Investigation, L.Z. and Z.X.; Data Curation, J.T. and B.M.; Writing-Original Draft Preparation, B.M., L.Z. and R.W.; Writing-Review & Editing, Z.X. and M.C.

**Funding:** This research was funded by the National Natural Science Foundation of China (No. 31401566 and 31601550), the National Key Technology Support Program (No. 2016YFF0203701), and the Natural Science Foundation of Hunan Province China (No. 2017JJ3150).

**Acknowledgments:** The authors are grateful to the National Natural Science Foundation of China, the National Key Technology Support Program and the Natural Science Foundation of Hunan Province China for providing the funding for this project. The authors thank Xiangtan University for the measurement. The authors thank Xiang Qi for their technical assistance.

**Conflicts of Interest:** The authors declare no conflict of interest.

## References


1. Diamanti-Kandarakis, E.; Bourguignon, J.-P.; Giudice, L.C.; Hauser, R.; Prins, G.S.; Soto, A.M.; Zoeller, R.T.; Gore, A.C. Endocrine-disrupting chemicals: An Endocrine Society scientific statement. *Endocr. Rev.* **2009**, *30*, 293–342. [CrossRef] [PubMed]
2. Bartrem, C.; Tirima, S.; Von, L.I.; Von, B.M.; Worrell, M.C.; Mohammad, A.S.; Abdullahi, A.; Moller, G. Unknown risk: Co-exposure to lead and other heavy metals among children living in small-scale mining communities in Zamfara State, Nigeria. *Int. J. Environ. Health Res.* **2014**, *24*, 304–319. [CrossRef] [PubMed]
3. Guerra, F.; Trevizam, A.R.; Muraoka, T.; Marcante, N.C. Heavy metals in vegetables and potential risk for human health. *Sci. Agric.* **2012**, *69*, 54–60. [CrossRef]
4. Tchounwou, P.B.; Yedjou, C.G.; Patlolla, A.K.; Sutton, D.J. Heavy Metal Toxicity and the Environment. In *Molecular, Clinical and Environmental Toxicology. Volume 3: Environmental Toxicology*; Luch, A., Ed.; Springer: Basel, Switzerland, 2012; pp. 133–164.
5. Zhang, W.; Xiong, B.; Chen, L.; Lin, K.; Cui, X.; Bi, H.; Guo, M.; Wang, W. Toxicity assessment of Chlorella vulgaris and Chlorella protothecoides following exposure to Pb(II). *Environ. Toxicol. Pharmacol.* **2013**, *36*, 51–57. [CrossRef] [PubMed]
6. Canário, C.; Ngobeni, P.; Katskov, D.A.; Thomassen, Y. Transverse heated filter atomizer: Atomic absorption spectrometric determination of Pb and Cd in whole blood. *J. Anal. At. Spectrom.* **2004**, *19*, 1468–1473. [CrossRef]
7. Narin, I.; Soylak, M. Enrichment and determinations of nickel(II), cadmium(II), copper(II), cobalt(II) and lead(II) ions in natural waters, table salts, tea and urine samples as pyrrolydine dithiocarbamate chelates by membrane filtration–flame atomic absorption spectrometry combination. *Anal. Chim. Acta* **2003**, *493*, 205–212.
8. Liu, R.; Liu, X.; Tang, Y.; Wu, L.; Hou, X.; Lv, Y. Highly sensitive immunoassay based on immunogold-silver amplification and inductively coupled plasma mass spectrometric detection. *Anal. Chem.* **2011**, *83*, 2330–2336. [CrossRef] [PubMed]
9. Elzinga, E.J.; Rouff, A.A.; Reeder, R.J. The long-term fate of $Cu^{2+}$, $Zn^{2+}$, and $Pb^{2+}$ adsorption complexes at the calcite surface: An X-ray absorption spectroscopy study. *Geochim. et Cosmochim. Acta* **2006**, *70*, 2715–2725. [CrossRef]
10. Taghdisi, S.M.; Danesh, N.M.; Lavaee, P.; Emrani, A.S.; Ramezani, M.; Abnous, K. A novel colorimetric triple-helix molecular switch aptasensor based on peroxidase-like activity of gold nanoparticles for ultrasensitive detection of lead(II). *RSC Adv.* **2015**, *5*, 43508–43514. [CrossRef]
11. Thomas, J.M.; Ting, R.; Perrin, D.M. High affinity DNAzyme-based ligands for transition metal cations—A prototype sensor for $Hg^{2+}$. *Org. Biomol. Chem.* **2004**, *2*, 307–312. [CrossRef] [PubMed]
12. Chen, G.; Guo, Z.; Zeng, G.; Tang, L. Fluorescent and colorimetric sensors for environmental mercury detection. *Analyst* **2015**, *140*, 5400–5443. [CrossRef] [PubMed]
13. Wu, X.; Tang, L.; Ma, W.; Xu, L.; Liu, L.; Kuang, H.; Xu, C. SERS-active Au NR oligomer sensor for ultrasensitive detection of mercury ions. *RSC Adv.* **2015**, *5*, 81802–81807. [CrossRef]
14. Wang, X.; Yang, C.; Zhu, S.; Yan, M.; Ge, S.; Yu, J. 3D origami electrochemical device for sensitive $Pb^{2+}$ testing based on DNA functionalized iron-porphyrinic metal-organic framework. *Biosens. Bioelectron.* **2017**, *87*, 108–115.
15. Frost, M.S.; Dempsey, M.J.; Whitehead, D.E. Highly Sensitive SERS Detection of $Pb^{2+}$ Ions in Aqueous Media using Citrate Functionalised Gold Nanoparticles. *Sens. Actuators B Chem.* **2015**, *221*, 1003–1008. [CrossRef]
16. Wu, L.; Xiao, X.; Chen, K.; Yin, W.; Li, Q.; Wang, P.; Lu, Z.; Ma, J.; Han, H. Ultrasensitive SERS detection of Bacillus thuringiensis special gene based on Au@Ag NRs and magnetic beads. *Biosens. Bioelectron.* **2017**, *92*, 321–327. [CrossRef] [PubMed]
17. Kang, Y.; Zhang, H.; Zhang, L.; Wu, T.; Sun, L.; Jiang, D.; Du, Y. In situ preparation of Ag nanoparticles by laser photoreduction as SERS substrate for determination of $Hg^{2+}$. *J. Raman Spectrosc.* **2017**, *48*, 399–404. [CrossRef]
18. Indrasekara, A.S.; Meyers, S.; Shubeita, S.; Feldman, L.C.; Gustafsson, T.; Fabris, L. Gold nanostar substrates for SERS-based chemical sensing in the femtomolar regime. *Nanoscale* **2014**, *6*, 8891–8899. [CrossRef] [PubMed]

19. Kabashin, A.V.; Evans, P.; Pastkovsky, S.; Hendren, W.; Wurtz, G.A.; Atkinson, R.; Pollard, R.; Podolskiy, V.A.; Zayats, A.V. Plasmonic nanorod metamaterials for biosensing. *Nat. Mater.* **2009**, *8*, 867–871. [CrossRef] [PubMed]
20. Li, J.; Chen, C.; Jans, H.; Xu, X.; Verellen, N.; Vos, I.; Okumura, Y.; Moshchalkov, V.V.; Lagae, L.; Van, D.P. 300 mm Wafer-level, ultra-dense arrays of Au-capped nanopillars with sub-10 nm gaps as reliable SERS substrates. *Nanoscale* **2014**, *6*, 12391–12396. [CrossRef] [PubMed]
21. Kim, J.H.; Han, S.H.; Chung, B.H. Improving $Pb^{2+}$ detection using DNAzyme-based fluorescence sensors by pairing fluorescence donors with gold nanoparticles. *Biosens. Bioelectron.* **2011**, *26*, 2125–2129. [CrossRef] [PubMed]
22. Lin, Z.Z.; Chen, Y.; Li, X.H.; Fang, W.F. $Pb^{2+}$ induced DNA conformational switch from hairpin to G-quadruplex: Electrochemical detection of $Pb^{2+}$. *Analyst* **2011**, *136*, 2367–2372. [CrossRef] [PubMed]
23. Lee, J.H.; Nam, J.M.; Jeon, K.S.; Lim, D.K.; Kim, H.; Kwon, S.; Lee, H.; Suh, Y.D. Tuning and Maximizing the Single-Molecule Surface-Enhanced Raman Scattering from DNA-Tethered Nanodumbbells. *ACS Nano* **2012**, *6*, 9574–9584. [CrossRef] [PubMed]
24. Ndokoye, P.; Ke, J.; Liu, J.; Zhao, Q.; Li, X. L-Cysteine-Modified Gold Nanostars for SERS-Based Copper Ions Detection in Aqueous Media. *Langmuir* **2014**, *30*, 13491–13497. [CrossRef] [PubMed]
25. Shao, N.; Jin, J.Y.; Cheung, S.M.; Yang, R.H.; Chan, W.H.; Mo, T. A Spiropyran-Based Ensemble for Visual Recognition and Quantification of Cysteine and Homocysteine at Physiological Levels. *Angew. Chem.* **2006**, *45*, 4944–4948. [CrossRef] [PubMed]
26. Xu, L.G.; Zhao, S.; Ma, W.; Wu, X.L.; Li, S.; Kuang, H.; Wang, L.B.; Xu, C.L. Multigaps Embedded Nanoassemblies Enhance in Situ Raman Spectroscopy for Intracellular Telomerase Activity Sensing. *Adv. Funct. Mater.* **2016**, *26*, 1602–1608. [CrossRef]
27. Yan, W.J.; Xu, L.G.; Xu, C.L.; Ma, W.; Kuang, H.; Wang, L.B.; Kotov, N.A. Self-Assembly of Chiral Nanoparticle Pyramids with Strong R/S Optical Activity. *J. Am. Chem. Soc.* **2012**, *134*, 15114–15121. [CrossRef] [PubMed]
28. Wang, T.; Hu, X.; Dong, S. Surfactantless synthesis of multiple shapes of gold nanostructures and their shape-dependent SERS spectroscopy. *J. Phys. Chem. B* **2006**, *110*, 16930–16936. [CrossRef] [PubMed]
29. Kim, Y.K.; Ok, G.; Choi, S.W.; Jang, H.; Min, D.H. The interfacing structural effect of Ag/graphene oxide nanohybrid films on surface enhanced Raman scattering. *Nanoscale* **2017**, *9*, 5872–5878. [CrossRef] [PubMed]
30. Zhu, J.; Li, J.J.; Zhao, J.W. The Effect of Dielectric Coating on the Local Electric Field Enhancement of Au-Ag Core-Shell Nanoparticles. *Plasmonics* **2015**, *10*, 1–8. [CrossRef]
31. Chai, F.; Wang, C.; Wang, T.; Li, L.; Su, Z. Colorimetric detection of $Pb^{2+}$ using glutathione functionalized gold nanoparticles. *ACS Appl. Mater. Interfaces* **2010**, *2*, 1466–1470. [CrossRef] [PubMed]
32. Roy, L.E.; Martin, L.R. Theoretical prediction of coordination environments and stability constants of lanthanum lactate complexes in solution. *Dalton Trans.* **2016**, *45*, 15517–15522. [CrossRef] [PubMed]
33. Wang, Z.P.; Ding, S.D.; Hu, X.Y.; Li, S.M.; Su, D.P.; Zhang, L.R.; Liu, Y.; Jin, Y.D. Selective extraction of americium(III) over europium(III) ions in nitric acid solution by NTAamide(C8) using a novel water-soluble bisdiglycolamide as a masking agent. *Sep. Purif. Technol.* **2017**, *181*, 148–158. [CrossRef]
34. Bahta, A.; Parker, G.A.; Tuck, D.G. Critical survey of stability constants of complexes of thiocyanate ion. *Pure Appl. Chem.* **1997**, *69*, 1489–1548. [CrossRef]
35. Polavarapu, L.; Perez-Juste, J.; Xu, Q.H.; Liz-Marzán, L.M. Optical sensing of biological, chemical and ionic species through aggregation of plasmonic nanoparticles. *J. Mater. Chem. C* **2014**, *2*, 7460–7476. [CrossRef]
36. Jiang, C.; Guan, Z.; Lim, S.Y.; Polavarapu, L.; Xu, Q.H. Two-photon ratiometric sensing of $Hg^{2+}$ by using cysteine functionalized Ag nanoparticles. *Nanoscale* **2011**, *3*, 3316–3320. [CrossRef] [PubMed]